Journal of Power Sources 266 (2014) 353–364

Contents lists available at ScienceDirect

Journal of Power Sources

journal homepage: www.elsevier.com/locate/jpowsour

The use of well-aligned composite nanorod arrays as anode material for lithium rechargeable batteries

B.D. Polat, O. Keles*

Department of Metallurgical and Materials Engineering, Istanbul Technical University (ITU), Maslak, Istanbul 34469, Turkey

HIGHLIGHTS

- Oblique angle electron beam deposition is used to form well-aligned CuSi nanorods.
- The adhesion of the film is improved by a prior deposition of the non porous film.
- The nanocolumnar morphology improves the electrochemical performance of the anode.
- XPS analyses reveal changes in SEI depending on the thin film's states of charge.
- An electrochemical dilatometer is first used to measure the volumetric changes.

ARTICLE INFO

Article history:
Received 13 January 2014
Received in revised form
26 April 2014
Accepted 3 May 2014
Available online 14 May 2014

Keywords:
Lithium ion battery
Nanorod
Composite thin film
Oblique angle deposition

ABSTRACT

The relations between the morphology and electrochemical performance of the thin film anodes made of copper and silicon are investigated. A well-aligned nanorods containing composite thin film and a composite thin film with no alignment in its structure are fabricated by electron beam deposition. Galvanostatic half-cell measurements show that the well-aligned anode exhibits a longer cycle life with a moderate capacity due the particularities in its composition, structure and morphology: Cu in the films buffers the mechanical stress occurred during lithiation and the existence of amorphous and nano-sized particles enhances cycleability. Moreover, the nanorods formation in the thin film increases the contact area of the anode with Li and decreases the polarization on the electrode surface. Plus, the homogenously distributed nano-sized interspaces among these nanorods enhance the mechanical tolerance of the electrode against volumetric changes.

In this work, the electrodilatometric analysis is also accomplished to measure the volumetric changes occurred upon cycling of the well-aligned nanorods containing thin film anode, and the difference in the electrochemical performances of the composite films resulting from different substrate position versus crucible is evaluated based on the X-ray photoelectron spectroscopy (XPS) analysis on the cycled samples.

1. Introduction

A development on the lithium ion battery (LIB) technology is highly required to improve the use of the effective energy storage devices. Within this concept, there is a great commercial interest in developing advanced electrode material. Knowing that negative electrode is the main contributor to the cell's overall electrochemical performance and silicon (Si) is one of the most abundant elements on earth, this study focuses on improving electrochemical performance of Si based materials used as negative electrode material in LIB. In fact, it is well known that the large volume expansion (400%) encountered during the alloying of Si with Li and the eventual pulverization of anode is the main disadvantage of the Si based anode materials, which restricts their wide usage in LIB.

To enhance the use of such Si based electrodes, researchers investigate the effects of electrode compositions and microstructural morphologies [1]. In literature, to provide a longer cycle life to an electrode, some scientists add a limited amount of copper (Cu) into silicon (Si) anode [2,3]. Cu is particularly chosen, because it has a superior conductivity and good solubility in Si, which in turn improves the electrical conductivity as well as the mechanical flexibility of the deposited film and its binding to Cu current collector [4]. However, deciding the amount of Cu added into the Si anode is

* Corresponding author. Tel.: +90 212 285 3398; fax: +90 212 285 3427.
E-mail addresses: ozgulkeles@itu.edu.tr, b.denizpolat@gmail.com (O. Keles).

http://dx.doi.org/10.1016/j.jpowsour.2014.05.006
0378-7753/

a challenging task. Because, even though Cu increases the cycleability of the Si anode for the above mentioned reason, the theoretical capacity of the anode decreases due to electrochemically inactive behavior of Cu. Therefore, an optimization about the Cu content has been done previously, where the best result has been achieved by forming 90%at.Si–10% at.Cu containing anode material. In addition to this, recently, some researchers work on decreasing the particle size of the electrode [5–7] because it is believed that a nano-sized composite anode will have a higher electrochemical performance. However, during cycling, the nanoparticles merge due to their high surface energy (electrochemical sintering) to form dense blocks which are unable to take part in the electrochemical reaction [8]. Therefore, the particle–particle interaction in the electrode material should be avoided not only compositionally but also geometrically.

The production of Cu–Si nanorods in thin films could prevent "the electrochemical sintering" problem, due to their unique morphology. The interstitial space among these nanostructures (nanorods) is expected to avoid sintering and minimize macroscopic mechanical stresses arising during the insertion and removal of Li^+, so as to preserve electrode integrity. Moreover, these free spaces among the nanorods provide large active sites to accommodate lithium (Li^+) and generate an easy route for the electrolyte to access the entire anode surface, which in turn improves capacity delivered by electrodes [9,10]. In 2011, Ryu et al. prove that the nanostructured electrodes improve the cycle life (nanorod's diameter < 300 nm) because of the fast Li^+ diffusion, which reduces polarization and creates small stresses along the film upon cycling [9].

So far, in order to have Si nanorods, laser irradiation of silicon surface [11], chemical vapor deposition of SiH_4 [12,13] and lithography based ion etching methods [14] were used. Oblique angle deposition (OAD) via electron beam evaporation method has also taken attention. Because in such an evaporation method, it is possible to avoid the hazardous flammable handling, explosive or cancerogenous metal nanoparticles. In addition, OAD enables direct deposition of the well-aligned inclined nanorods on a current collector, eliminating the need of binder or conductive additives to get homogeneously distributed porosities in thin films, which ensures the direct transportation of electrons; hence a fast Li^+ diffusion through their controllable, small diameters [15].

The mechanism of the nanorods formation during the OAD method has been studied previously. The results show that it is possible to control the orientation of the nanorods growth by changing the incident flux angle because the electron beam deposition is a line-of sight process. Therefore, to have nanorods in OAD method, the substrate position should be fixed to receive the evaporated particle flux under a highly oblique angle (Θ) of the substrate's surface normal ($\Theta > 70^\circ$). The vapor flux ($\vec{F}$) hits the substrate from both vertical ($\vec{F}_I = \vec{F}\cdot\cos\theta$) and lateral ($\vec{F}_{//} = \vec{F}\cdot\sin\theta$) directions: the vertical component ($\vec{F}_I$) induces film growth and the lateral component ($\vec{F}_{//}$) contributes to the shadowing effect [15].

Karabacak et al. [16,17] highlight the importance of this "shadowing effect" and define it as one of the dominated mechanism that controls the oblique angle deposition, competing with "surface diffusion process". At room temperature deposition, since the surface diffusion rate is very slow, the impinging atoms randomly form islands on the substrate, when such growth is governed by Volmer–Weber or Stranski–Krastanov process. As deposition proceeds, the initially nucleated islands act as shadowing centers and all large islands receive more impinging atoms as compared to small ones, leading to inclined nanocolumnar film growth, where homogeneously distributed porosities are formed among the inclined nanorods. Thereby, a decrease in the incident flux angle (Θ) deteriorates the columnar growth, and generates a non-aligned (flat) film when the Θ is 0°. Thus, to control the porosity or interspaces the incident flux angle (Θ) should be close to 90°.

Table 1
EDS analyses of the non-aligned and the well-aligned nanorods containing Cu–Si composite thin films.

Non-aligned Cu–Si thin film				Nanorods containing well-aligned Cu–Si thin film			
Cu		Si		Cu		Si	
at%	wt%	at%	wt%	at%	wt%	at%	wt%
11.46	22.67	88.53	77.33	8.81	17.94	91.19	82.06

Besides the incident flux angle (Θ), substrate surface roughness and evaporation source composition have significant impacts on the composition and the morphology of thin films, which in turn affect their electrochemical performances, when used as anodes in LIB [15–17].

Cracking, pulverization and peeling of the Si based thin film from the underlying current collector during cycling test are major problems encountered when Si based films used as anodes. In literature, different methodologies have been proposed to resolve these problems: one is to engineer a nanostructured compliant layer below or above thin films to reduce the stress [17], another is to engineer a graded composition through the films [18].

In this study, the oblique angle electron beam co-evaporation method is used to produce well-aligned Cu–Si nanorods containing thin film. In order to enhance the electronic contact of the thin film with the substrate and to delay aggregation in the thin film during cycling, first a layer of Ref. [16] a non-aligned (flat) Cu–Si layer is deposited before the well-aligned nanorods as it has been done in our previous work [19]. Furthermore, to compare the electrochemical performances, a thin film with no alignment in its structure is also produced. XPS analyses of both anodes at different states of charges (pristine, 1st discharge and 1st charged states) are also done to discuss the changes in the electrode/electrolyte interfaces of the films, depending on their morphologies. Finally, an in-situ electrochemical dilatometer is used to measure the volumetric change occurred in the first cycles of the well-aligned nanorods containing composite thin film. Among alternative measuring techniques (in-situ neutron images taken during cycling [20], in-situ strain gauge [21], in-situ X-ray [22] measurements and atomic force microscopy [23]) we particularly choose this method because it gives accurate information about non-periodic strain similar to that in amorphous phases or on the surface of the material.

2. Experimental

The non-aligned and the well-aligned Cu–Si nanorods containing thin films were deposited on copper discs (with 15.5 mm diameter and 1.5 mm thickness) using electron beam co-deposition technique. In addition to copper (Cu) discs, a pure silicon (Si) wafer (20×10 mm^2) and a stainless steel (SS) disc (15.6 mm diameter and 1 mm thickness) were also coated during the experiments, to measure the coating thickness, and the composition of the thin films accurately. It should be emphasized that the Cu and Si pellets were put together in a graphite crucible prior to the co-evaporation deposition process, where their ratio (Cu/Si weight ratio) was 1:9, for each sample.

During the experiment, first a non-aligned thin film was deposited on a Cu substrate with an incident flux angle of 0°. Then, the well-aligned composite nanorods were formed when the deposition flux hit onto the substrate surface's normal with an angle of 80° at room temperature.

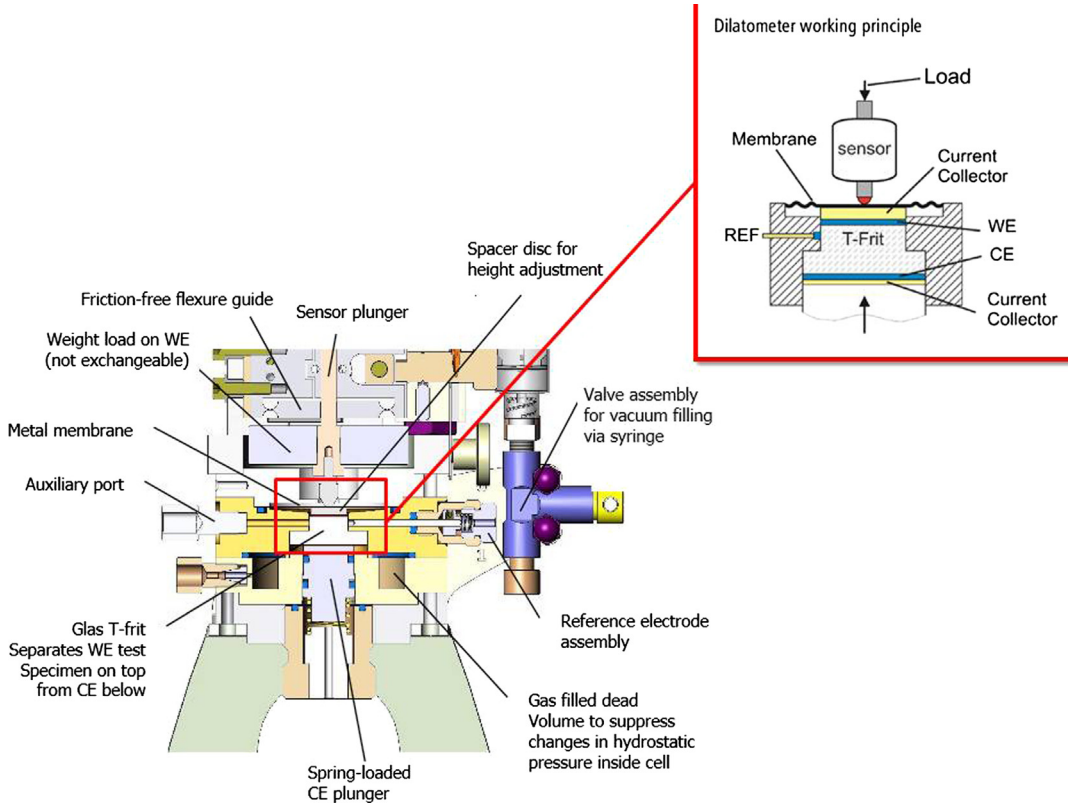

Fig. 1. Schematic representation of electrochemical dilatometer (ECD-nano).

The deposition flux was constant (4 Å s^{-1}) during the overall process and the base pressure in the vacuum chamber was 10^{-7} Pa.

The composition of the film was determined by energy dispersive X-ray spectroscopy (Oxford, EDS) analysis (Table 1). The weight of the thin film was measured by using (My weight i101) microbalance before and after the coating process. Moreover, the active material weight in the thin films was found by multiplying the total weight of the coating with the weight percentage of the active material determined through EDS analyses (Table 1). This value was then used to calculate the specific capacity delivered by anode materials.

The surface morphologies of the anodes before and after the electrochemical tests and the thin film thicknesses were looked at by utilizing a field-emission scanning electron microscopy (FE-SEM, JEOL-JSM-7000F and JEOL-5410). The surface roughness of thin films prior to electrochemical analyses was also observed via atomic force microscopy (AFM, with Digital Instrument (DI) Controller IV under dimension 3100 platform). The phases exist in the pristine were determined using Philips-PW3710 System with a 2θ range of 20–100 in steps of 0.05 (with CuKα at 40 kV and 30 mA).

Half cells were assembled as 2032 coin cells, in an argon-filled glove box (Mbraun, Labmaster) with thin films as test electrodes, pure Li foil as counter electrode, and porous polypropylene film (Celgrad 2400) as separator. The non-aqueous electrolyte used during the experiments was 1 M $LiPF_6$ dissolved ethylene carbonate (EC) and dimethyl carbonate (DMC) in a 1:1 weight ratio. The cells were tested at room temperature and operated at voltages of 50 mV–2.5 V versus Li/Li^+ with a rate of 50 mA g^{-1}. Cyclic voltammetry (CV) was performed in the potential range of 50 mV–2.5 V versus Li/Li^+ at a scan rate 0.03 mV s^{-1} for the first 3 cycles; and electrochemical impedance spectroscopy (EIS) was accomplished in frequency range of 10 mHz–10,000 Hz at 1.2 V with 5 mV rms after the 1st and the 25th cycles (Gamry pci 4/750).

To determine the chemical state of the elements present on the pristine electrodes' surfaces and investigate the charge–discharge products formed during the 1st cycle, XPS analyses were performed on the pristine, the 1st discharged and the 1st charged electrodes by using a Kratos™ Axis Ultra DLD surface analysis instrument. The samples were prepared for the XPS analyses by disassembling the coin cells in an argon-filled glove box (Mbraun, Labmaster) and washed with DMC to remove the salt from the electrode surfaces. Prior to introduction into the load-lock vacuum chamber of the XPS instrument, all air-sensitive samples were loaded into an inert transfer module interfaced with a particular instrument. The samples were prepared in an argon-filled glove box, with no more than 1 ppm O_2 and 1 ppm H_2O. The base pressure of the analysis chamber during these experiments was 3×10^{-10} Torr, with operating pressures around 10^{-9} Torr. Spectra were collected with a monochromatic Al Kα source (1486.7 eV) and a 300 × 700 micron spot size. Peak position was further corrected by referencing the C1s peak position of adventitious carbon for a sample (284.8eV, *PHI Handbook of Photoelectron Spectroscopy*), and shifting all other peaks in the spectrum accordingly. Data fitting was done by using the program CasaXPS. Each relevant spectrum was fit to a Shirley type background to correct for the rising edge of backscattered electrons which shifted the baseline higher at high binding energies. Peaks were fitted as asymmetric Gaussian/Lorentzians, with 0–30% Lorentzian character.

Finally, we measured the expansion occurred in the well-aligned Cu–Si nanorods containing thin film electrode by an electrochemical dilatometer [24]. The schematic representation of ECD-nano was given in Fig. 1. The cell of the electrochemical dilatometer was given with a closure view on the right side of Fig. 1. The dilatometer cell contained two electrodes (working electrode and lithium) separated by a glass frit. An aluminum foil current collector was placed on the top of the working electrode to transmit any

height change to a sensor/load unit placed at the top of the cell. The dilatometer cell was filled with electrolyte in the argon-filled glove box (Mbraun, Labmaster). Before the test, a mechanical load of 1 N was applied onto the working electrode, then measurements were performed in a temperature controlled cabinet with the rate of 200 mA g^{-1} between 50 mV and 2.5 V. The test cabinet at a constant temperature (29 ± 0.1 °C) and any gas evolution was prevented by connecting the cell to atmospheric pressure via a capillary tube (0.1 mm inner diameter, 1m length).

3. Results and discussion

The surface and the cross sectional views of the non-aligned structured and the well-aligned nanorods containing Cu–Si thin films are shown in Fig. 2a–d. From the top view, a homogenous morphology is noticed for both samples (Fig. 2a and c). The thickness of the non-aligned thin films is observed to be around 100 nm (Fig. 2b). On the other hand, the SEM image shown in Fig. 2d reveals that the well-aligned and tilted Cu–Si nanorods have approximately 20 nm of diameters and 100 nm of lengths. The presence of the nano-sized interspaces among these nanorods form homogenously distributed porosities (interspaces) in the well-aligned structured thin film, as seen in Fig. 2c. This regular alignment of the nanorods, which leads to porosities, not only facilitates the electrolyte penetration and increases the accessible surface area of the anode to react with lithium but also decreases the polarization and enhances the mechanical tolerance against the volumetric change occur during cycling. On the other hand, the non-aligned thin film is made of small sized particles, packing closely to each other, which in turn limits the reaction of Li^+ with the surface of the anode material (see Fig. 2a). In Table 1, EDS analyses reveal that both films contain similar amount of silicon, approximately 90%at. independent from their morphologies.

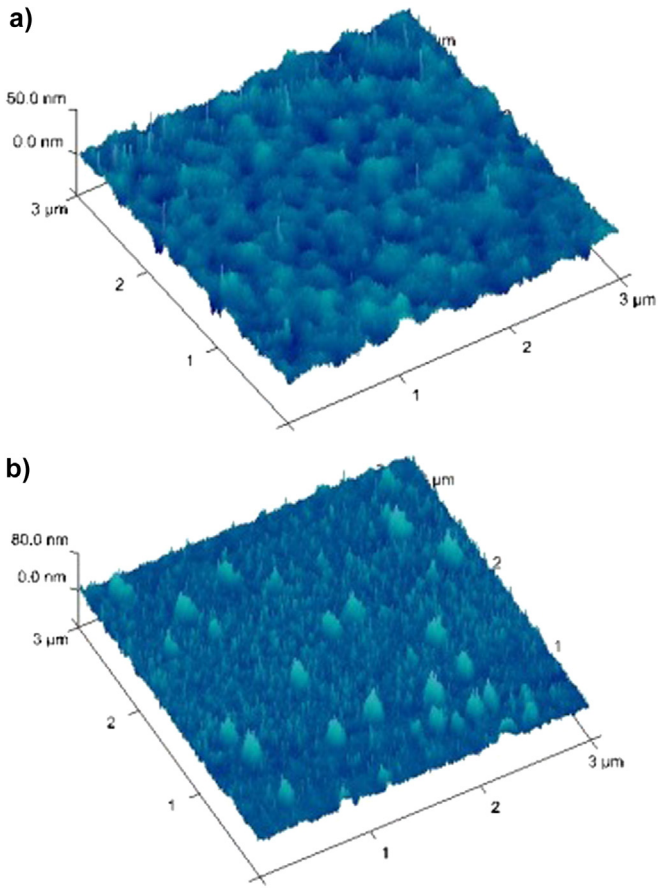

Fig. 3. AFM images of (a) the non-aligned structured, (b) the well-aligned nanorods containing Cu–Si thin films.

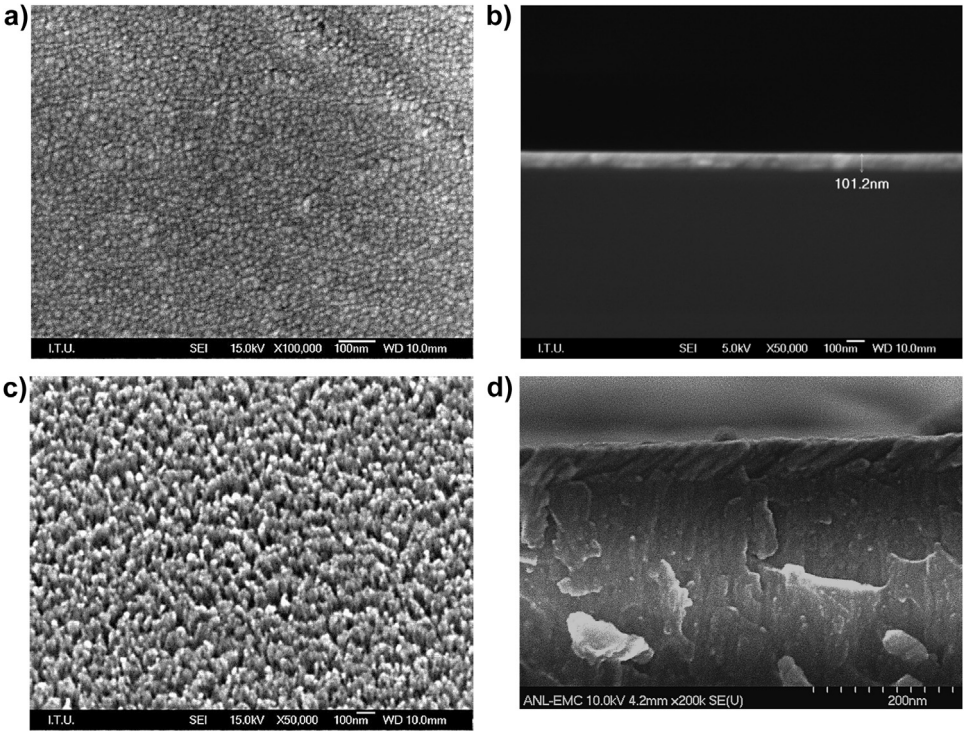

Fig. 2. FE-SEM (a) the surface (b) the cross sectional images of the non-aligned structured film, and (c) the surface (d) the cross sectional images of the well-aligned nanorods containing composite Cu–Si thin films.

Furthermore, AFM analyses justify in Fig. 3a and b that the surface roughness of the electrodes changes depending on the presence of the well-aligned nanorods in the thin film. The formation of the homogenously distributed Cu–Si nanorods issued from the restricted and the directed growth of the thin film, forms a high surface roughness as seen in Fig. 3b. The non-aligned structured Cu–Si thin film has 4.85 nm whereas the well-aligned nanorods containing Cu–Si thin film has 8.27 nm surface roughness.

The structural properties of the electrodes are further investigated by means of XRD (Fig. 4).

Knowing that the film thickness has an influence on the structure of the electrode, films with a thickness around 100 nm are fabricated in this work to minimize the crystallization and the agglomeration of particles during the deposition [25]. Thereby, the formation of amorphous and nano-sized crystalline phases noted on both samples can be considered as an outcome of the experimental parameters (Fig. 4). Additionally, both electrodes demonstrate the presence of polycrystalline orthorhombic Cu_3Si particles, which are one of the reasons for the improved electrochemical performances of these anodes compared to that of the pure Si. Moreover, the XRD data of the well-aligned nanorods containing Cu–Si thin film demonstrates a Si peak at 56.122°, which is originated from the Si wafer since there is no such a peak detected in the XRD data of the well-aligned Cu–Si nanorods containing thin film formed on a Cu disc (the data is not given here).

The existence of the nanocrystalline (α-Si) and amorphous (a-Si) Si particles is very critical for the electrochemical performances of the electrodes since their reactions with Li^+ differentiate, depending on the cell potential [26]. In previous studies, the fundamental understanding of their Li^+ insertion/extraction mechanisms was analyzed by using in-situ XRD, SEM and high resolution transmission electron microscopy (HR-TEM) [26–29]. The results show that during Li^+ insertion, the crystal structure of the nano-sized Si particle is destroyed and converted into an amorphous metastable structure (Li–Si) according to the "solid-state amorphization theory" [28,29], without formation of any intermediate phase. This amorphous lithiated Si phase prevails up to 0.05 V, then a new crystalline compound ($Li_{15}Si_4$) is formed when the cell potential decreases to lower values ($V < 0.05$ V). Furthermore, during Li^+ extraction crystalline (on the anodic side) $Li_{15}Si_4$ is converted into both amorphous and crystalline particles, where an internal trapping of Li^+ ion occurs, resulting in a decrease in the specific capacity delivered. On the other hand, Li^+ insertion into an amorphous Si anode forms an amorphous lithiated Si product, which is converted into $Li_{15}Si_4$ at a voltage lower than 0.05 V. Seeing that any lattice expansion could be adequately prevented by eliminating the formation of the two phases, the latter proves the advantageous of using amorphous Si particles, since Li^+ diffusion paths are developed in the amorphous thin film, leading to a higher electrochemical performance.

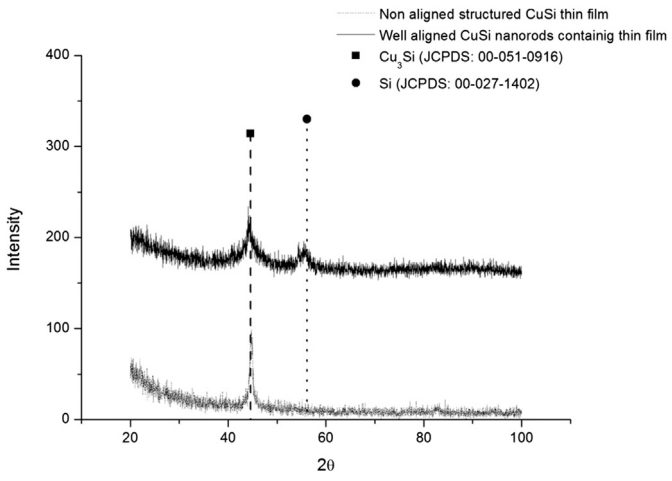

Fig. 4. XRD patterns of the as-deposited non-aligned and the well-aligned structured Cu–Si thin films.

Moreover, the comparison of the characteristic peak of the Cu_3Si phase ($2\Theta = 44.57°$) proves that both films are made of nano-sized particles but the aligned one has smaller sized Cu_3Si crystallites as the characteristic peak is broader on its spectrum. Herein, the nano-sized Cu_3Si presence on both thin films is very important since it is believed that the high electronic conductivity of the Cu_3Si alloy promotes a good interparticles electronic conduction, which in turn suppresses the Si volume changes effectively. In Equation (1), the reaction mechanism of the Cu_3Si with Li^+ is shown: the elemental Cu formed during the first lithiation reaction would act as a buffering matrix to minimize the destroying effect of the volume changes due to Li_xSi formation (Equation (1)). This lithiated Si product surrounded in the conductive Cu matrix enhances the reversibility of the charge/discharge reactions, which intensifies the cycle stability of the electrode, eventually [26,30].

$$xLi^+ + xe^- + Cu_3Si \rightarrow Li_xSi + 3Cu \rightarrow 3Cu + Si + xLi^+ + xe^- \quad (1)$$

The Li^+ insertion/removal into the non-aligned and the well-aligned thin films are investigated by CV tests, for the first 3 cycles (Fig. 5a and b). The peaks obtained are attributed to the potential dependent formation and disappearance of Li_xSi alloys of different compositions and structures. The comparison between Fig. 5a and b reveals that the current-potential characteristics of the non-aligned film are slightly different from that of the well-aligned nanostructured Cu–Si film. Moreover, clear differences in the curvature shapes between the first and the subsequent cycles are noted for the non-aligned thin film (Fig. 5a), where a high capacitance effect is remarkably recognized, due to the restricted Li^+ diffusion by the electrode surface. The first discharge (Li alloying) process of the non-aligned film shows three cathodic peaks at the potentials of 0.8, 0.5 and 0.25 V (Fig. 5a). The first cathodic peak (around 0.8 V) is attributed to the formation of the solid electrolyte interface (SEI) since it disappears after the 1st cycle; and the other two represent the reduction reactions of Si and SiO_2 particles, to form lithiated products (such as Li_xSi and Li_2O [31]). No SiO_2 peak is detected in the XRD data of the thin films. The presence of the CV peak shows the reduction reaction of SiO_2 with Li^+ might be explained by the nano-sized morphology of SiO_2 particles formed due to a possible oxidation of underlying Si atoms in the thin film. The anodic peak detected at about 1.2 V shows the oxidation during the delithiation reaction. After the 1st cycle, the cathodic peak around 0.8 V disappears. The CV curves of the 2nd and 3rd cycles are highly overlapped where a broad cathodic peak around 0.6 V, and a sharp peak at 0.08 V are displayed. This proves that an irreversible reaction is suppressed by maintaining the equilibrium state after the 1st cycle, because some reactions go on the non-aligned Cu–Si film, although the SEI film prevails after the first discharge reaction.

On the other hand, the CV curvatures of the well-aligned Cu–Si nanorods containing thin film (Fig. 5b) prove that a low capacitive effect exists on the nanostructured electrode surface, thus Li^+ diffusion is not limited by the surface reaction, it can diffuse through the bulk material during the cycle test. When the current-potential characteristics of the well-aligned thin film for the first 3 cycles are compared, variations in the number of peaks and their intensities are noted. The CV curvature of the as-deposited film displays one small and one remarkable reduction peaks around

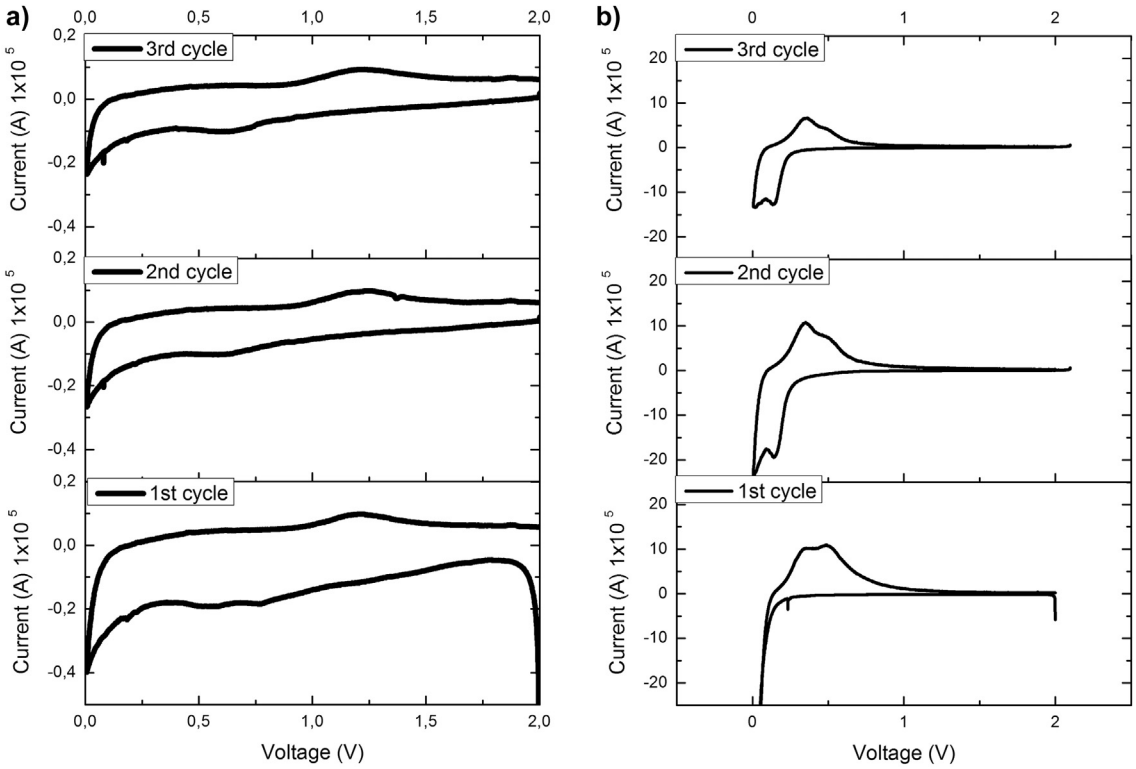

Fig. 5. First 3 cycles' cyclic voltammetry of (a) the non-aligned and (b) the well-aligned nanorods containing Cu–Si thin films.

0.25 V and 0.1 V respectively. These peaks demonstrate the lithiation of SiO_2 and nano-sized/amorphous Si particles during the first discharge reaction, respectively. Then, during the extraction of Li^+, two anodic peaks (around 0.3 and 0.5 V) showing the partial recovery of Si particles form the Li_xSi particles are detected on the surface of the electrode [25]. In this regard, it is reasonable to consider that a reduction peak indicating the SEI formation on the anode surface is included in the cathodic peak around 0.1 V, since the intensities of cathodic peaks are decreased in following cycles. This decrease in peak intensities might prove the prevalence of an irreversible reaction on the electrode surface, in the presence of SEI film (Fig. 5b).

When Fig. 5b is examined in detail, a decrease in the intensity of the sharp peak around 0.1 V and the formation of an additional peak around 0.2 V in the following cycles are noticed. The possible phase change of the nanostructured Si thin film might explain this additional peak formation [32].

When the current intensities appeared on the CV profiles of both films after the 1st and 3rd cycles are compared, a significant reduction of cathodic peaks is clearly seen. Xianhua et al. [33] indicate that among all Li–Si intermetallics, the ones having less Li (LiSi, $Li_{12}Si_7$) have the highest formation energy, thus the highest stability compared to others (Equations (2) and (3)). Once, one of these Li deficient intermetallics are formed (LiSi, $Li_{12}Si_7$), it will be difficult to dissociate them due to their high stability [34].

$$xLi^+ + Si_{(crystalline)} + xe^- \rightarrow Li_xSi_{(amorphous)} \quad (2)$$

$$Li_xSi_{(amorphous)} \rightarrow (x-y)Li^+ + Li_ySi_{(amorphous)} + (x-y)e^- \quad (3)$$

Fig. 6a and b shows the reversible capacity delivered by the electrodes. The curves are typical for the reaction of Si with Li, which suggest that Cu is inactive versus Li^+ [35]. In the 1st cycle both anodes perform a large amount of irreversible capacity. The lower irreversible capacity loss noted in following cycles reflects that the irreversible reaction mainly takes place in the 1st cycle. Knowing that all the reduction reactions above 0.8 V decomposes the electrolyte, the change in slope appeared around 0.8 V (versus Li/Li^+) is likely associated to SEI formation, which may account for some portion of the irreversible capacity (200 mAh g^{-1} for the non-aligned and 880 mAh g^{-1} for the well-aligned nanorods containing thin films).

Fig. 6a and b also exhibit a small slope at 0.8 V in the 2nd–5th cycles. This outcome is in agreement with the CV test results where the prevalence of SEI is highlighted. Therefore, the formation of the SEI layer is very critical. Although it causes a drastic reduction in the charge consumption at the beginning, it enhances the reversibility of lithium intercalation/deintercalation reactions (93% and 99% coulombic efficiency for the non-aligned and well-aligned thin films, respectively). Another reason for a drastic reduction in the capacity (around 40% coulombic efficiency), besides SEI layer, trapped Li^+ in the two phase regions as a result of the lithiation reactions of Si nano-sized crystals or an irreversible formation of Li^+ deficient Si phases depending on the cell potential [33,34].

Furthermore, EIS spectra of both films show one semi-circle at high frequency region (Fig. 7a and b), which shows the adsorption of Li^+. Moreover, the information on the transport of the adsorbed species along the structure might be obtained by examining the curvature shape in the smaller frequency range [36]. In addition, the existence of the upward slope at the low frequency region also provides information on Li^+ diffusion into the anode material. In view of that, a comparative EIS analysis of both electrodes is accomplished. On the 1st cycle EIS data of the thin film with no alignment in its structure shows low Li^+ diffusion since the capacitive behavior limits Li^+ reaction with the film surface, which in turn deviates the slope at low frequency region far away from 45°. When the capacitive behavior of the non-aligned anode is distorted due to high volumetric change, an inclined slope with 45°

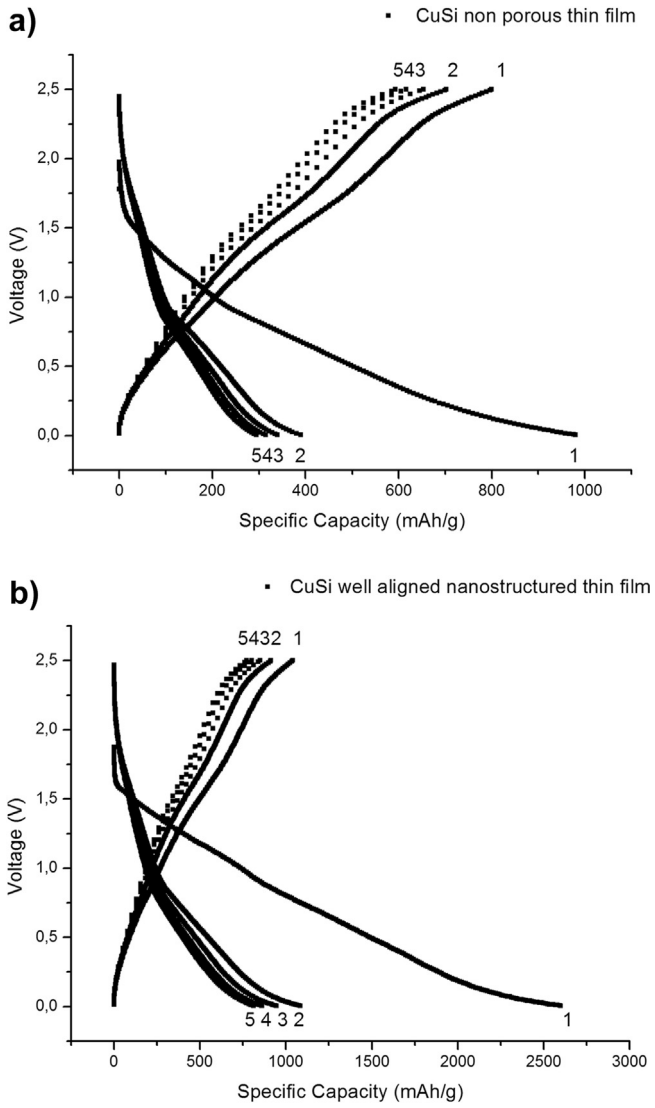

Fig. 6. Voltage profiles of (a) the non-aligned and (b) the well-aligned nanorods containing Cu–Si thin films for the first 5 cycles, with 50 mA g^{-1} current rate.

is found in Fig. 7a, which demonstrates that very limited amount of Li^+ starts to diffuse through the films after the 25th cycles. On the other hand, the slopes seen on the EIS data of the 1st and the 25th cycles of the well-aligned nanorods containing thin film (at low frequency region) are close to 45°, justifying that Li^+ can diffuse through the bulk material during the whole cycle test. Plus, the comparison in the arc diameter of both films after the 1st and the 25th cycles displays a decrease. It is possible to explain this change considering the "electrochemical grinding" which is resulted from Ref. [37] the low mechanical resistance of the thin film against the high volumetric change in cycling. In this regard, once the average particle size is reduced in the films; the surface area of the anode is increased. The high surface area upturns the current passes in the cell and decreases the impedance detected from the anode. In this case, the Li^+ diffusion becomes easier and a better capacity utilization occurs with a higher columbic efficiency. Moreover, a decrease in the impedance of both electrodes in further cycles also proves the presence of the "SEI glue effect", which provides electrical conduction among the electrochemically grounded particles, resulted from the high volume changes. Since no binder is used during the electron beam deposition process, a possible delamination of the small particles from the current collector is mostly prevented due to the "SEI glue effect" which makes the SEI formation critical for the electrochemical behaviors of the porous composite films. Fig. 8a and b demonstrates the XPS analyses of the pristine, the 1st discharged and the 1st charged samples of both electrodes. It should be underlined that the absence of the binder in these anodes allows for a more straightforward analysis of the SEI formation and the changes in the anodes' surfaces.

The XPS spectra show some changes on both electrodes' surfaces after the 1st discharge and the 1st charge reactions (Fig. 8a and b). On the pristines; the C peak associated with the universal contamination, Si and Cu peaks are also detected. In addition, XPS spectra of Si2p show the presence of SiO_2 and Si(II) on the top layer of the non-aligned and well-aligned nanorods containing electrodes respectively. These peaks disappear by sputtering the surfaces with Ar^+ for 5 min. Moreover, the well-aligned structured pristine anode demonstrates $Cu(OH)_2$ presence on the top layer.

When the first discharged samples of both thin films are investigated, XPS analyses reveal no Si or Cu peaks, which proves that the SEI layer is thick enough to cover the electrode surface, and also SEI does not contain metallic Si at discharged state. Besides, when the SEI layer composition is investigated deeply on the discharged electrodes, XPS analyses reveal Li–F, C–F, Li–CO_3, O–C=O, C–C and C=O peaks on their data. Plus, a peak associated to M–O presence is also detected on thin films surfaces.

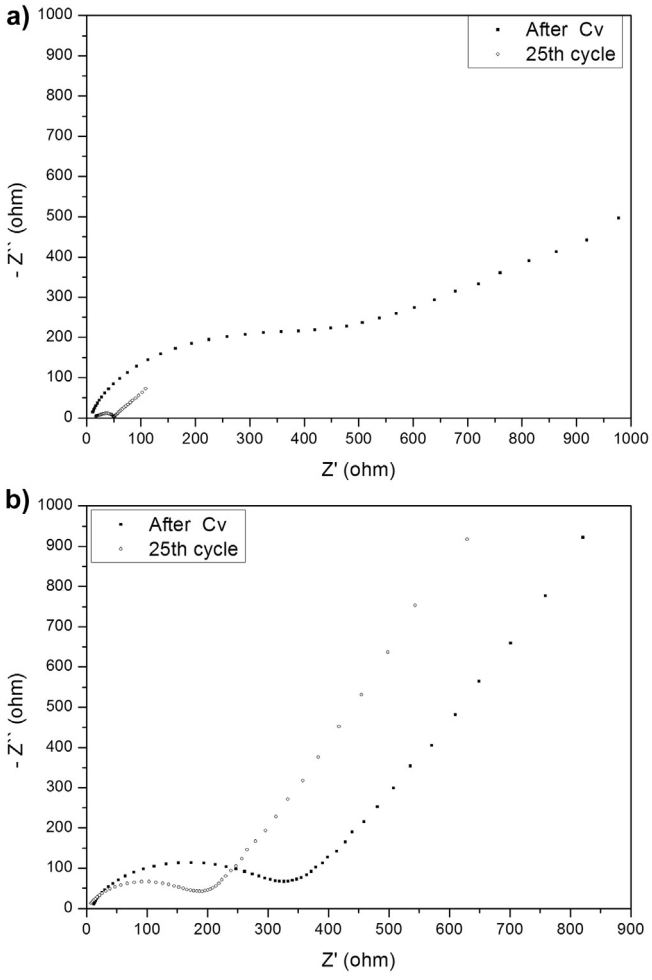

Fig. 7. Electrochemical impedance spectroscopy of (a) the non-aligned and (b) the well-aligned nanorods containing Cu–Si thin films after the 1st and the 25th cycles.

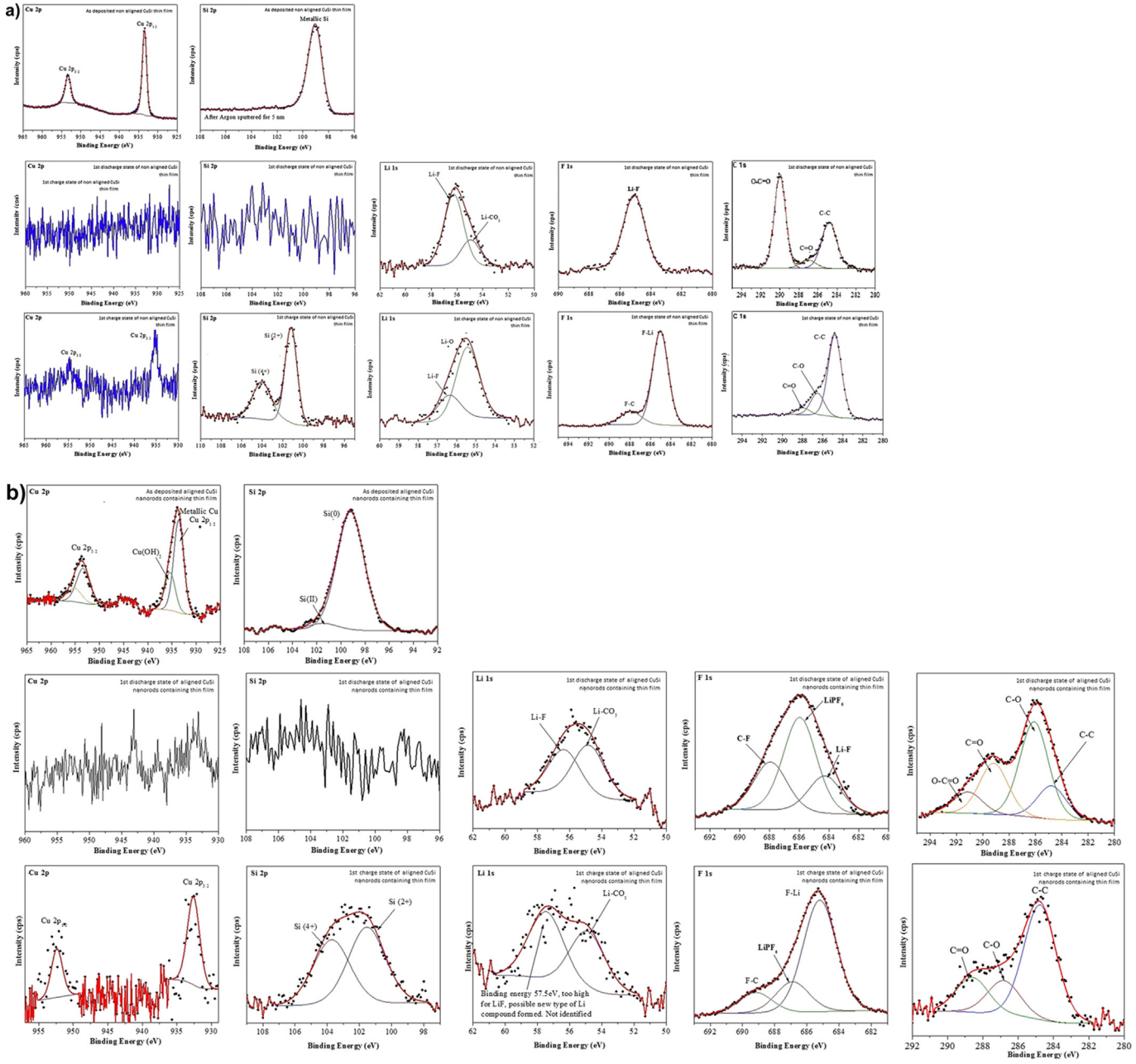

Fig. 8. XPS spectra of Cu 2p, Si 2p, Li 1s, and F1s peaks of (a) the non-aligned and (b) the well-aligned Cu–Si electrodes as pristines, after the first discharge and charge reactions.

Upon cycling, C1s and L1s spectra show some differentiation on both electrodes. The disappearance of O–C=O peaks on both charged anodes indicates the decomposition of lithium carbonate species under the charging process since C1s peak at 290.1 eV is assigned to the carbonate containing functionalities [38–40]. However, the prevalence of C–C, C–O, C=O peaks justifies the presence of the SEI layer on both charged anodes. In this sense, Schroder et al. [38] who deeply investigate those peaks seen on C1s spectra of Si anode, indicate that C1s peaks detected around 285.5–289 eV (C–C, C–O and O–C=O) might demonstrate the presence of PEO (polyethylene oxide) or ether functionalities or lithium alkoxides formed on the charged anode. These compounds could be derived from a one electron reduction of DEC or EC or carbonate products, which are further reduced to form ether, alkoxide, ester, carboxylate and the lithium oxide products of the SEI present on the anode. In addition, Fig. 8a and b also reveal small amounts of Cu peaks on both charged anodes and no metallic Si peaks are noted [30–32]. In addition, Si is present in the oxide film as Si^{2+} and Si^{4+}, representing that the SEI has some products containing Si^{2+} and Si^{4+} based materials such as Li_xSiO_y (Li_4SiO_4, Li_2SiO_3, $Li_6Si_2O_7$) [33], which is resulted from the irreversible reaction of SiO_2 with lithium upon discharge. Kim et al. [31] justify the presence of these compounds by using solid-state ^{29}Si- and ^{7}Li-nuclear magnetic resonance (NMR) methods and explain their formation considering the irreversible capacity lost of the electrode during cycling.

Our XPS findings (Fig. 8a and b) are similar to those previously reported for the Si thin film, Si nanowires, and Si nanoparticles. They reveal that the SEI is primarily composed of the electrolyte reduction products and contains low amount of Si due to irreversible reactions. The amount of Cu in the thin films seems to have

no effect on the SEI film formation as it is inactive to Li^+. Hence, it is believed that the role of Cu on the electrochemical performance of the anodes is mostly a "buffering". The XPS analyses are fully in agreement with the results of the electrochemical analyses (Figs. 5a, b and 6a, b). The SEI composition is independent of the thin film morphology and depends mostly on the electrolyte concentration and its additives. In our study, as we use a $LiPF_6$-EC based electrolyte, the XPS data of both electrodes are similar. Once the SEI forms, it prevails on the electrode in the subsequent cycles and suppresses the pulverization of small Si particles due to its "glue effect". Nie et al. [41] observe the SEI formation on the Si anode surface after several cycles by TEM analyses, which are also in line with our observations.

Fig. 9a and b displays the capacity-cycle performance of the non-aligned and the well-aligned Cu–Si thin films' along with their coulombic efficiencies. The capacity value in the graph is calculated based on the active material present in the thin films. Thus, when the theoretical capacities of the films based on EDS quantification are calculated $3579 \times 0.77 = 2755.8$ and $3579 \times 0.82 = 2934.7$ mAh g^{-1} for the non-aligned and the well-aligned nanorods containing Cu–Si thin films, respectively

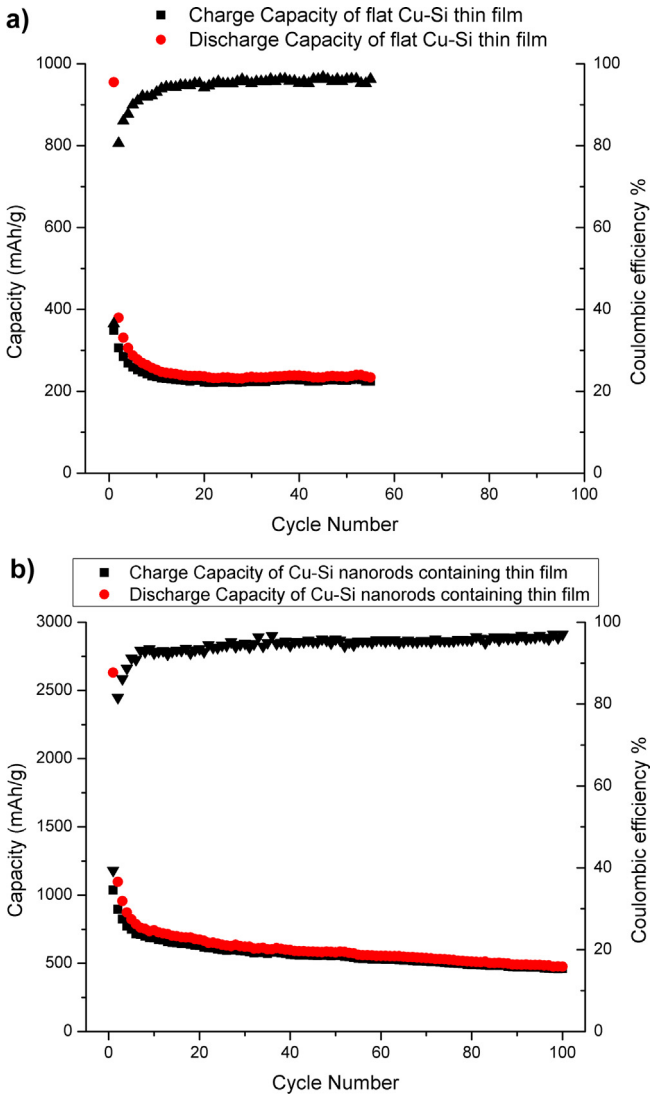

Fig. 9. Discharge capacity, charge capacity and Coulombic efficiency are plotted as a function of cycle numbers for (a) the non-aligned and (b) well-aligned nanorods containing Cu–Si thin films.

(3579 mAh g^{-1} is the theoretical capacity of Si assuming the formation of $Li_{3.75}Si$ and the fractions are those provided in Table 1). From these values, it is possible to rationalize that the use of OAD is very important to produce high electrochemical performance Cu–Si thin film, since even both films have the same composition, for the non-aligned composite thin film 950 mAh g^{-1} is measured as the first discharge capacity value, which represents 34% of its theoretical capacity; whilst with OAD method 2600 mAh g^{-1} is measured initially for the well-aligned structured anode, which is 89% of its theoretical capacity.

The low initial discharge capacity value (950 mAh g^{-1}) of the non-aligned Cu–Si thin film might result from the limited reactions of Li^+ with the active material (as shown in Fig. 6a, the capacitive effect of the thin film restricts the lithiation of the electrode by surface reactions due to its non-aligned morphology), and the irreversible reaction of Li^+ with Si and SiO_2 nano-sized particles present on the electrode surface. On the other hand, the high first discharge capacity of the well-aligned Cu–Si thin film can be justified considering the presence of amorphous particles, which provides a high accessible surface area for Li^+ to react with Si and lead to form homogeneously distributed porosities to suppress the volumetric change occurred during lithiation/delithiation.

When the cycleability of the electrodes is compared, it is seen that the non-aligned thin film delivers 200 mAh g^{-1} with 98% coulombic efficiency, upto 60 cycles. Then, the sample is failed, due to the delamination of the thin film, resulted from the uncovered volumetric changes. On the other hand, the well-aligned nanorods performs 550 mAh g^{-1} during 100 cycles, with approximately 99% Coulombic efficiency. This improved cycleability of the thin film can be related to the morphological and structural particularities.

While the existence of SiO_2 and nano-sized Si crystals adversely effects the electrochemical performance, the non-aligned layer

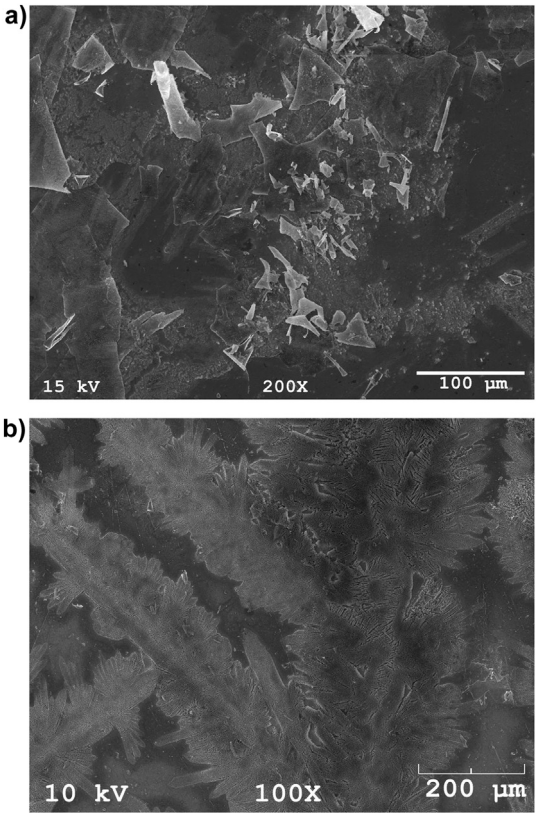

Fig. 10. FE-SEM images of (a) the non-aligned and (b) the well-aligned nanorods containing aligned Cu–Si thin film, after cycling test.

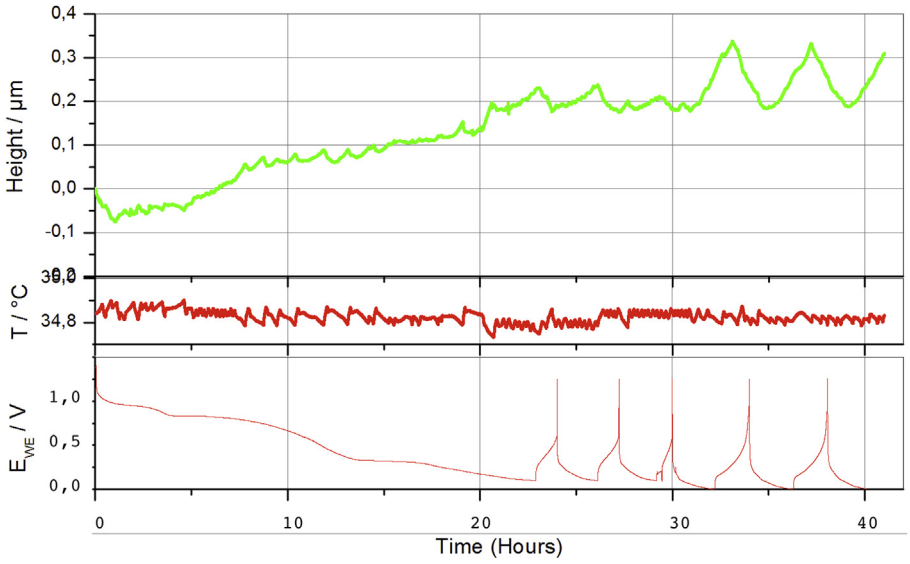

Fig. 11. An in-situ electrochemical dilatometer result for the well-aligned nanorods containing Cu–Si thin film.

prior to nanorods, amorphous particles, Cu atoms and homogenously distributed porosities improve the performance. As mentioned previously, during lithiation nano-sized Si crystals form a two phase region leading to a high internal stress in the thin film, which causes some amount of Li^+ trapped in the anode; but then, the reaction of amorphous particles with Li^+ results in the formation of an amorphous lithiated Si compounds (one phase), which in turn augments the cycle reversibility. Moreover, Cu_3Si intermetallics formed as a result of the co-evaporation of Cu with Si buffer the mechanical stress occurred during the lithiation process and increase the electrical conductivity among particles. Furthermore, the presence of the homogenously distributed nano-sized porosities decreases the polarization and increases the mechanical tolerances of the thin film. In addition, the existence of this primarily deposited non-aligned layer that works as a transition zone between the substrate and the composite nanorods, promotes the adhesion of the thin film to the current collector. And finally, the SEI layer "glue effect" gathering all the small electrochemically grounded particles of the thin film together could also explain the remarkable electrochemical performance of the well-aligned electrode for 100 cycles.

Herein, it is worth to note that even though the first discharge capacities of the electrodes are different, both perform similar initial coulombic efficiencies around 40%. The Li^+ trapping in the thin film electrode, the SEI covering the anode surface or the Li^+ deficient intermetallics formation after the first lithiation causing irreversible reactions with Si could explain this low coulombic efficiency. The development of the SEI on the well-aligned Cu–Si nanorods containing thin film could be rationalized considering its AFM analysis result. Because Fig. 3b shows clearly that the presence of nanorods in the thin film increases the surface roughness that enhances the surface reactivity of the electrode, leading to promote the reaction of the thin film with the electrolyte.

Fig. 10a and b demonstrates SEM views of both thin films after the cycling test. The images reveal that in the case of the non-aligned Cu–Si thin film, a severe delamination is clearly detected leading to a short cycle life (60 cycles) (see Fig. 10a), whilst on the well-aligned nanorods containing composite thin film, small sized cracks are formed with partial electrochemical grinding (see Fig. 10b).

To verify our explanation about the improved electrochemical behavior of the well-aligned Cu–Si nanorods containing thin film, an in-situ electrodilatometric measurement is undertaken, where the volumetric change versus time and the ambient temperature are registered during the galvanostatic test (Fig. 11).

So far, numerous works have been made on the volumetric change of the anodes by utilizing dilatometric analysis. Among them, in 2009, Camer et al. [35] produce Si and Si/C composite anodes using powder metallurgy. The results show that the composite electrodes have better capacity retention than that of pure nano Si. In 2011, Jeong et al. [42] produce Si based anodes having various porosity levels by using PMMA (polymethyl methacrylate) as a pore-forming agent and display the volumetric changes occurred in those anodes during cycling test. They found that the generation of additional pores alleviates the movement of Si-alloyed particles. A breakdown in the electrical network of the electrode makes an improvement in cycle performance. So far, there is no work in literature where the volumetric changes of a well-aligned nanostructured composite thin film anode formed via OAD method has been made by using in-situ electrochemical dilatometry.

It is worth to note that, main factors for volumetric changes in Si based anodes are composition and porosity. During the experiment, the sample having the composition of 90%at.Si, 10%at.Cu and the thickness of ~100 nm is analyzed. Knowing that this well-aligned thin film is made of nano-sized particles and amorphous structure (Fig. 3), the expansion is expected to be isotropic. Thus, the measured height change is believed to show the volumetric change in the thin film during the cycle test. The initial decrease in the height value noted in Fig. 11 during the rest period is due to the creeping of the dilatometer itself.

The potential profile and the simultaneous dilatation track recorded during the first lithiation show that the observed potential slopes may be attributed to the stoichiometry domains of pure intercalation phases, while the potential plateaus are related to the co-existence of two phases. Consequently, electrode swelling should primarily occur during the potential plateaus, and the associated height change can be calculated accordingly. Here, it is assumed that the volume expansion is accommodated by the height change since lateral expansion is prevented by the substrate. Thereby, Fig. 11 displays that during the 1st cycle, the formation of

SEI layer (around 0.8 V), the lithiation of SiO_2 (around 0.25 V) and Si (<0.2 V) particles, all cause swelling of the electrode. However, it is seen that the height change generated during the formation of SEI and the low density lithium silicates (Li_xSiO_y) followed by the lithiation of SiO_2 particles form less volume expansion [31].

Moreover, by analyzing the dilation behavior of the electrodes, reversibility in the dimensional change in each cycle is observed. The height change of the electrode proves that the expansion occurred in the first discharged reaction is not recovered totally by the electrode during the initial delithiation. This fact justifies that some amount of Si particles embedded in the thin film during discharge and can not be recovered during charge reaction, leading to a low coulombic efficiency. As explained previously, the formation of SEI or highly stable Li_xSi (or lithium silicates) phases or Li trapping in the electrochemically grounded thin film could be reasons for this low coulombic efficiency. The electrode displays a stable dilation behavior only after the 3rd cycles, reflecting that this volume change is associated with the lithiation and delithiation of Si particles during cycling test. Because the formation of Li_xSi particles having lower densities [31] induces more stress in the thin film, which in turn increases the height of the thin film at discharged state. Herein, it is highly believed that unlike Si electrodes, the residual dilation state at the end of the 3rd cycle is reduced due to the presence of copper and homogeneously distributed porosities in the thin film [42].

In addition, the change of the height versus the ambient temperature is also observed in Fig. 11, where a remarkable correlation between the temperature change and the dilatation is noted. This thermal expansion is mainly that of the dilatometer itself, rather than that of the film, which justifies our sensitivity to keep the temperature stable during the experiment.

When necessary calculation is done a height drift of 6.5 nm h^{-1} is found through the electrochemical dilatometer analysis, which proves that 200% volumetric change occurs when the well-aligned nanorods containing Cu–Si thin film is used as anode material in LIB. The presence of Cu and homogeneously distributed porosities presence are believed to be reasons for this remarkable performance.

The result of ECD-nano test justifies the reason of the low initial coulombic efficiency of the nanostructured electrode and demonstrates that compared to that of pure Si film [43], an improvement in the volumetric expansion is achieved when a well-aligned nanorods containing Cu–Si thin film is used as anode in LIB.

4. Conclusion

In this study, we demonstrate that the well-aligned Cu–Si nanorods containing thin film can be fabricated by a practical method called OAD in an e-beam physical vapor deposition system.

Outcomes of the study are summarized as follows:

- The use of OAD is very important to produce high electrochemical performance Cu–Si thin film, since even both films have the same composition, for the non-aligned composite thin film 950 mAh g^{-1} is measured as the first discharge capacity value, which represents 34% of its theoretical capacity; whilst with OAD method 2600 mAh g^{-1} is measured initially, which is 89% of its theoretical capacity.
- XPS analyses verify that the reduction reaction of the electrolyte on the anode surface occurs for both anodes. The repeated volume expansion and contraction of the nanoparticles in further cycles results in significant increases in the concentration of the electrolyte decomposition products and consequences remarkable changes in the silicon containing nanoparticles properties. The changes in the surface properties of the thin film electrodes are reflected as a continuous decrease in the capacity performance of the anodes in initial cycles, and then stabilization is noticed when the oxide film is well established at the electrode–electrolyte interface.
- A 6.5 nm h^{-1} average height drift was detected by electrochemical dilatometer (ECD-nano) for initial cycles of the well-aligned Cu–Si nanorods containing thin film. The height change versus cell voltage displays that during the 1st cycle, the formation of SEI layer and the lithiation of SiO_2 and Si particles, all cause swelling of the electrode. However, it is seen that the height change generated during the formation of SEI and the low density lithium silicates (Li_xSiO_y) followed by the lithiation of SiO_2 particles form less volume expansion, compared to that of the Si particles.
- Larger particle size with highly crystalline particles and the absence of porosities in the non-aligned thin film deliver poor electrochemical performance. Cu atoms, amorphous and nano-sized Si based particles presence forming the aligned nanorods which generate homogenously distributed nano-sized porosities as interstitial spaces among them are the major reasons for the improved cycleability of the aligned anode material.

Acknowledgment

Authors thank Dr. Khalil Amine, Dr Daniel Abraham, Dr. Ali Abouimrane, and Dr Hatice Karahan for their support in improving the paper; and appreciate Prof. Dr. Gültekin Göller, Hüseyin Sezer, Talat Alpak, Dr Matthias Hahn and Dr. Jun Lu for their supports to accomplish the FE-SEM, electrodilatometer and XPS investigations.

References

[1] M. Au, Y. He, Y. Zhao, H. Ghassemi, R.S. Yassar, B.G. Diaz, T. Adams, J. Power Sourc. 196 (2011) 9640–9647.
[2] J.W. Kim, J.H. Ryu, K.T. Lee, S.M. Oh, J. Power Sourc. 147 (2005) 227–233.
[3] J.P. Maranchi, A.F. Hepp, A.G. Evans, N.T. Nuhfer, P.N. Kumta, J. Electrochem. Soc. 153 (2006) A1246–A1253.
[4] M.M. Thackeray, J.T. Vaughey, C.S. Johnson, A.J. Kropf, R. Benedek, L.M.L. Fransson, K. Edstrom, J. Power Sourc. 113 (2003) 124–130.
[5] Z. Wen, S. Huang, X. Yang, B. Lin, Solid State Ionics 179 (2008) 1800–1805.
[6] S. Huang, Z. Wen, X. Zhu, X. Yang, J. Electrochem. Soc. 152 (2005) A1301–A1305.
[7] Y. Oumellal, N. Delpuech, D. Mazouzi, N. Dupré, J. Gaubicher, P. Moreau, P. Soudan, B. Lestriez, D. Guyomard, J. Mater. Chem. 21 (2011) 6201–6208.
[8] N. Dimov, S. Kugino, M. Yoshio, Electrochim. Acta 48 (2003) 1579–1587.
[9] I. Ryu, J.W. Choi, Y. Cui, W.D. Nix, J. Mech. Phys. Solids 59 (2011) 1717–1730.
[10] T. Umeno, K. Fukuda, H. Wnag, N. Dimov, T. Iwao, M. Yoshio, Chem. Lett. 30 (2001) 1186–1187.
[11] O.T. Ghalehbeygi, V. Kara, L. Trabzon, S. Akturk, H. Kizil, Nano Res. 16 (2011) 15–20.
[12] C. Chan, H. Peng, G. Liu, K. McIlwrath, X.F. Zhang, R. Huggins, Y. Cui, Nat. Nanotechnol. 3 (2008) 31–35.
[13] H. Chen, Y. Xiao, L. Wang, Y. Yang, J. Power Sourc. 196 (2011) 6657–6662.
[14] D. Zschech, D.H. Kim, A.P. Milenin, R. Scholz, R. Hillebrand, C.J. Hawker, T.P. Russell, M. Stienhart, U. Gosele, Nano Lett. 7 (2007) 1516–1520.
[15] Y. He, Y. Zhao, Nanoscale 3 (2011) 2361–2375.
[16] D.X. Ye, T. Karabacak, R.C. Picu, G.C. Wang, T.M. Lu, Nanotechnology 16 (2005) 1717–1723.
[17] T. Karabacak, J. Appl. Phys. 96 (2004) 5740–5746.
[18] Y. He, J. Fan, Y. Zhao, Cryst. Growth Des. 10 (2010) 4954–4958.
[19] B.D. Polat, N. Sezgin, O. Keles, K. Kazmanlı, A. Abouimrane, K. Amine, J. Alloy Compd. 553 (2013) 204–207.
[20] J.B. Siegel, A.G. Stefanopoulou, P. Hegans, Y. Ding, D. Gorsich, J. Electrochem. Soc. 160 (8) (2013) A1031–A1038.
[21] X. Wang, Y. Sone, G. Segami, H. Naito, C. Yamada, K. Kibe, J. Electrochem. Soc. 154 (1) (2007) A14–A21.
[22] I.A. Courtney, J.R. Dahn, J. Electrochem. Soc. 144 (1997) 2045–2052.
[23] H. Wu, Y. Cui, Nano Today 7 (2012) 414–429.
[24] M. Hahn, O. Barbieri, F.P. Campana, R. Kötz, R. Gallay, Appl. Phys. 82 (2006) 633–638.
[25] T.D. Hatchard, J.R. Dahn, J. Electrochem. Soc. 151 (2004) A838–A842.
[26] U. Kasavajjula, C. Wang, A.J. Appleby, J. Power Sourc. 163 (2007) 1003–1039.
[27] H. Li, X. Huang, L. Chen, H. Zhou, Z. Zhang, D. Yu, Y.J. Mo, N. Pei, Solid State Ionics 135 (2000) 181–191.

[28] P. Limothongkul, Y.-I. Jang, N.J. Dudney, Y.-M. Chiang, J. Power Sourc. 119–121 (2003) 604–609.
[29] P. Limothongkul, Y.-I. Jang, N.J. Dudney, Y.-M. Chiang, Acta Mater. 51 (2003) 1103–1113.
[30] R.D. Thomson, K.N. Tu, Phys. Lett. 41 (1982) 440–443.
[31] T. Kim, S. Park, S.M. Oh, J. Electrochem. Soc. 154 (12) (2007) A1112–A1117.
[32] M.N. Obravac, L.J. Krause, J. Electrochem. Soc. 154 (2007) A103–A108.
[33] H. Xianhua, S. Hu, Q. Ru, Z. Zhang, Rare Metals Mat. Eng. 39 (2010) 2079–2083.
[34] L. Jing, J.R. Dahn, J. Electrochem. Soc. 154 (2007) A156–A161.
[35] J.L.G. Camer, J. Morales, L. Sanchez, P. Ruch, S.H. Ng, R. Kötz, P. Novak, Electrochim. Acta 54 (2009) 6713–6717.
[36] C. Wang, A.J. Appleby, F.E. Little, Electrochim. Acta 46 (2001) 1793–1813.
[37] Y. Liang, S. Yang, Z. Yi, X. Lei, J. Sun, Y. Zhou, Mat. Sci. Eng. B 121 (2005) 152–155.
[38] K.W. Schroder, H. Celio, L.J. Webb, K.J. Stevenson, J. Phys. Chem. C. 116 (2012) 19737–19747.
[39] D. Dees, E. Gunen, D. Abraham, A. Jansen, J. Prakash, J. Electrochem. Soc. 152 (2005) A1409–A1417.
[40] B. Philippe, R. Dedryvere, J. Allouche, F. Lindgren, M. Gorgio, H. Rensmo, D. Gonbeau, K. Edström, Chem. Mater. 24 (2012) 1107–1115.
[41] M. Nie, D.P. Abraham, Y. Chen, A. Bose, B.L. Lucht, J. Phys. Chem. C. 117 (2013) 13403–13412.
[42] G. Jeong, S.M. Lee, N.S. Choi, Y.U. Kim, C.K. Lee, Electrochim. Acta 56 (2011) 5095–5101.
[43] M. Holzapfel, H. Buqa, L.J. Hardwick, M. Hahn, A. Würsig, W. Scheifele, P. Novák, R. Kötz, C. Veit, F.M. Petrat, Electrochim. Acta 52 (2006) 973–978.